Computers in Biology and Medicine 134 (2021) 104476

Contents lists available at ScienceDirect

Computers in Biology and Medicine

journal homepage: www.elsevier.com/locate/compbiomed

The electrocardiographic forward problem: A benchmark study

Jake A. Bergquist [a,b,c,1], Wilson W. Good [a,b,c,1], Brian Zenger [a,b,c,d,*,1], Jess D. Tate [a], Lindsay C. Rupp [a,b,c], Rob S. MacLeod [a,b,c,d]

[a] Scientific Computing and Imaging Institute, University of Utah, SLC, UT, USA
[b] Nora Eccles Cardiovascular Research and Training Institute, University of Utah, SLC, UT, USA
[c] Department of Biomedical Engineering, University of Utah, SLC, UT, USA
[d] School of Medicine, University of Utah, SLC, UT, USA

ARTICLE INFO

Keywords:
Electrocardiographic forward problem
Electrocardiographic imaging
Cardiac electrophysiology
Experimental cardiac electrophysiology
Experimental validation
Cardiac bioelectricity

ABSTRACT

Background: Electrocardiographic forward problems are crucial components for noninvasive electrocardiographic imaging (ECGI) that compute torso potentials from cardiac source measurements. Forward problems have few sources of error as they are physically well posed and supported by mature numerical and computational techniques. However, the residual errors reported from experimental validation studies between forward computed and measured torso signals remain surprisingly high.

Objective: To test the hypothesis that incomplete cardiac source sampling, especially above the atrioventricular (AV) plane is a major contributor to forward solution errors.

Methods: We used a modified Langendorff preparation suspended in a human-shaped electrolytic torso-tank and a novel pericardiac-cage recording array to thoroughly sample the cardiac potentials. With this carefully controlled experimental preparation, we minimized possible sources of error, including geometric error and torso inhomogeneities. We progressively removed recorded signals from above the atrioventricular plane to determine how the forward-computed torso-tank potentials were affected by incomplete source sampling.

Results: We studied 240 beats total recorded from three different activation sequence types (sinus, and posterior and anterior left-ventricular free-wall pacing) in each of two experiments. With complete sampling by the cage electrodes, all correlation metrics between computed and measured torso-tank potentials were above 0.93 (maximum 0.99). The mean root-mean-squared error across all beat types was also low, less than or equal to 0.10 mV. A precipitous drop in forward solution accuracy was observed when we included only cage measurements below the AV plane.

Conclusion: First, our forward computed potentials using complete cardiac source measurements set a benchmark for similar studies. Second, this study validates the importance of complete cardiac source sampling above the AV plane to produce accurate forward computed torso potentials. Testing ECGI systems and techniques with these more complete and highly accurate datasets will improve inverse techniques and noninvasive detection of cardiac electrical abnormalities.

1. Introduction

Accurate assessment of cardiac electrical activity is essential to diagnose and treat many cardiac diseases. There are several methods to measure this activity, directly through invasive contact mapping of the endocardial or epicardial surfaces; and indirectly through noninvasive means such as 12-lead electrocardiography, body surface potential mapping, and electrocardiographic imaging (ECGI) [1–3]. Of these methods, ECGI has shown significant promise clinically to noninvasively and quantitatively reconstruct cardiac electrical potentials [1,4–7]. ECGI uses body surface recordings, geometric models, and biophysical mathematical relationships to compute epicardial, endocardial, or intramural cardiac signals.

A crucial component of ECGI is the mathematical relationship describing cardiac bioelectric sources and how they project through an electrically passive torso volume, known as the electrocardiographic

* Corresponding author. 72 Central Campus Dr, Salt Lake City, UT, 84112, USA.
E-mail address: brian.zenger@hsc.utah.edu (B. Zenger).
[1] These authors contributed equally to this research.

https://doi.org/10.1016/j.compbiomed.2021.104476
Received 15 March 2021; Received in revised form 2 May 2021; Accepted 3 May 2021
Available online 15 May 2021

forward problem. Solutions to this problem are determined from the specific bioelectric source model, the electrical conductivities of the tissue, and subject-specific anatomical models. Forward problems are generally well-posed biophysically and supported by mature mathematical formulations and numerical techniques. These favorable factors create expectations that the solutions to such problems can be very accurate, limited only by predictable factors such as model resolution, the accuracy of assumptions about tissue conductivities, and other model parameters. However, validation studies based on experimental measurements have reported significant errors between forward computed and measured body surface potentials [8–12].

Possible origins of error in the forward problem include the type of cardiac source representation, geometric errors in heart and torso geometries, incomplete or low-resolution cardiac source sampling, and inadequate representation of conductivity inhomogeneities in the torso. Bear et al. investigated the effects of incorporating inhomogeneous torso conductivities into the forward model [8]. Their study is one of the few that have reported the surprising errors associated with the forward problem and did so using a novel and elegant experimental preparation. Bear et al. also reported more accurate forward computed potentials by including tissue conductivity inhomogeneities in the formulation. However, the reported errors were still higher than expected for this forward problem, *i.e.,* correlation coefficients at approximately 0.8. Other, less precise experimental validation studies have reported a similarly high error in forward computed potentials and attributed the error to the limitations of imprecise geometries, incomplete sampling, *etc.* [9,11–18].

The source of forward problem error that we have targeted in this study was incomplete cardiac source sampling. Most experimental preparations described in the literature utilized an epicardial sock, strips of epicardial electrodes, or individual electrodes stitched onto the epicardium, all of which primarily sample the ventricular epicardium below the atrioventricular (AV) plane [8,12,19]. In our previous study, Tate et al. [9] investigated the error in the forward problem from incomplete or low-resolution sampling of the cardiac source using two simulated datasets and a coarsely sampled set of experimental results. The results suggested that incomplete cardiac source sampling resulted in significant errors in the forward computed potentials, particularly with incomplete sampling above the AV plane. However, the study was limited by coarse electrode spacing and experiments designed for a different purpose.

The results from Tate et al. led us to hypothesize that signals acquired above the AV plane are critical to sample the complete bioelectric source and construct accurate forward solutions. Specifically, we were interested in which measurements are required to achieve the expected high correlation (above 0.95) between measurements and forward solutions. To test this hypothesis, we used our modified Langendorff preparation, in which an isolated canine heart was suspended in a human-shaped, instrumented torso tank filled with conductive media and perfused from a second support animal. To this arrangement, we added a novel pericardial cage electrode array that captured the electrical activity of the isolated heart over a surface surrounding the entire heart. Using this experimental preparation, we examined how cardiac source sampling, specifically the coverage above the AV plane, contributed to errors in forward computed potentials using an pericardial potential cardiac source model. Additionally, our study generated datasets with unprecedented signal quality and forward problem accuracy that will create a new benchmark for both this forward problem and ECGI techniques.

2. Methods

2.1. Experimental preparation

The modified Langendorff preparation used in this study is similar to those described previously [20–22]. In short, an isolated canine heart was suspended in a human torso-shaped tank and perfused retrogradely via the aorta using a support animal (Fig. 1). The donor animals weighed approximately 25 Kg and the support animals weighed approximately 35 Kg and all dogs were over 6 months old. The torso tank was filled with electrolytic fluid made up of sodium chloride (0.023 mol/L), sucrose (0.26 mol/L), and deionized water with a target conductivity of 500 Ωcm to approximate the conductivity of the human torso [13,20]. Temperature in the torso tank was maintained at 37° C with heating pumps and countercurrent heat exchangers. Temperature in the torso tank was monitored continuously and the heating bath was adjusted to maintain a constant tank solution temperature. The support animal was maintained under general anesthesia and monitored frequently. Anesthesia was maintained using inhaled isoflurane between 1 and 5%. All animals were male and purpose-bred for use in experimental research, and all studies were approved by the Institutional Animal Care and Use Committee at the University of Utah and conformed to the Guide for Care and Use of Laboratory Animals (protocol number 17–04016 approved on 05/17/2017).

2.2. Pericardiac cage and tank electrode arrays

Electrical signals were recorded from the heart using a novel pericardiac electrode cage and the 384 embedded electrodes in the Utah torso tank. The Utah Pericardiac Cage (UPC) was a 3D-printed plastic, two-part frame into which 256 Ag/AgCl electrodes were embedded. The electrodes encircled the isolated heart roughly 1–2 cm from the epicardial surface. The electrodes were arranged to achieve consistent spacing over the surface and the result was a triangulated surface with an average triangular area of 84 mm^2 and an edge length of 21 mm. In the experiments, the two halves of the cage were placed around the isolated heart and rigidly suspended in the torso tank (see Fig. 2). The torso tank was modeled from an adolescent male torso (torso height 41 cm, depth 21 cm, and shoulder width 30 cm) and contained 384 Ag/AgCl electrodes from which we sampled 192 that formed a regularly spaced grid of 16 vertical columns of 12 electrodes each. All electrode recordings were referenced to Wilson's central terminal, which was constructed using three dedicated, embedded electrodes, one on each upper mid-axillary line and the floor of the tank, respectively. An example of the relative shape and spacing of the torso and cage arrays are shown in Fig. 1.

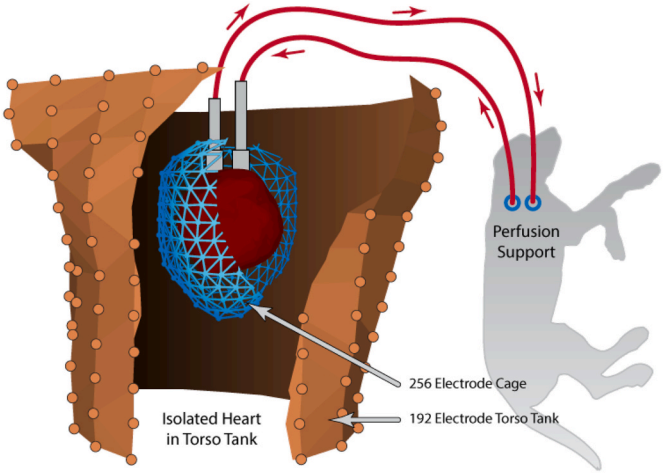

Fig. 1. The Utah Torso Tank preparation, based on modified a Langendorff perfusion system. A rigid pericardiac electrodes cage encircled the isolated heart, which was perfused from a second support animal through the aorta with blood returned under suction from the right ventricle. The human-torso-shaped tank was filled with electrolytic fluid consistent with human torso conductivity and sampled from 192 embedded Ag/AgCl electrodes. The recording system sampled cage and torso potentials simultaneously.

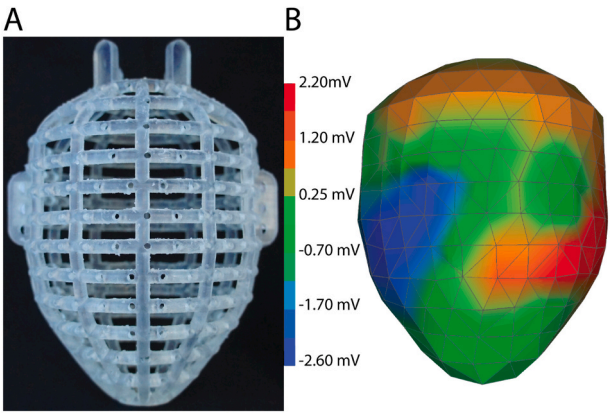

Fig. 2. The Utah Pericardiac Cage (UPC). Panel A: The UPC is a 3D printed 256-channel recording array. Two UPC halves are placed around the perfused, isolated heart, which is suspended in the torso tank. Panel B: The recorded signals can be mapped onto a digitized electrode geometry. Shown is an example potential measurement at 50% into the QRS complex of a sinus beat.

2.3. Signal acquisition equipment

A custom acquisition system recorded all electrical potentials simultaneously at a sampling rate of 1 kHz and 12-bit resolution [23]. The acquisition system consisted of variable gain input amplifiers, multiplexers, A/D converters, and interface circuitry, controlled by a personal computer via a custom LabVIEW (National Instruments, Austin, TX, USA) program to manage the hardware and continuously record signals.

2.4. Activation sequence types

For our analysis, we recorded three different activation sequence types: sinus rhythm and beats paced from bipolar needle electrodes in the anterior and posterior aspects of the left ventricular free wall (premature ventricular beats) (Fig. 3). The pacing in the LV freewall originated from near the epicardium and was maintained at a 171 bpm with 3-ms pulse duration and current set to two times threshold levels. The

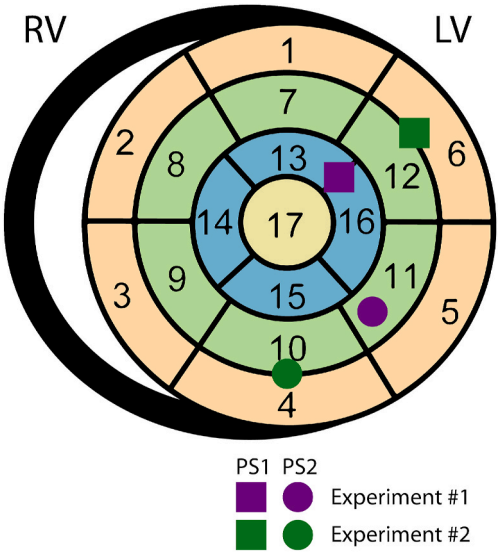

Fig. 3. Left Ventricular free wall pacing locations mapped on the American Heart Association 17-segment model. Pacing site one (PS1) is represented by boxes, pacing site two (PS2) is represented by circles, experiment one is represented as purple, and experiment two is shown in green. Note PS1 sites are in the anterior and PS2 sites in the posterior left ventricular (LV) free wall.

hearts beat with an intrinsic rhythm that was close to normal for canines, therefore, it was assumed to originate from an intact sinus node. We repeated these protocols in two experiments and from each experiment selected 40 beats per activation sequence type, resulting in 120 beats per experiment (240 beats in total) for analysis.

2.5. Signal processing

The recorded electrograms were processed using "Preprocessing Framework for Electrograms Intermittently Fiducialized from Experimental Recordings" (PFEIFER), an open-source MATLAB (The Mathworks Inc, Natick, Massachusetts) suite [24]. Using PFEIFER, all signals were filtered, baseline corrected, and fiducialized to mark standard time points within each electrogram or torso ECG. Our filtering use a weighted average approach with a window size of 11 and weights of a triangular shape as described previously [24]. Pacing artifacts were manually detected and interpolated using a cubic spline. Electrodes producing technically unacceptable signals on both the cage and torso recording arrays were also manually identified, eliminated, and reconstructed using Laplacian interpolation. Less than 25 torso-tank and 23 cage electrodes were identified for reconstruction for either experiment. Interpolated electrodes on the torso-tank surface were included in the statistical analyses. We selected 40 beats per activations sequence to assess the effect of beat to beat variability in forward computation. Template beats for each pacing site were manually fidicualized and subsequent matching beats (cross-correlation value above 0.98) were selected from up to a 90-s recording interval [24].

2.6. Geometric model

We modeled the pericardiac cage and torso-tank recording arrays as triangulated surfaces with each node corresponding to an electrode. Electrode locations were measured using a three-dimensional mechanical digitizer (Microscribe 3Dx, Immersion Corporation) and then triangulated manually to create cage and tank surface meshes. The cage mesh was rigidly transformed to the correct relative location and orientation within the torso tank using registration points recorded during the experiment.

The pericardiac cage was designed to minimize all possible sources of geometric error, *i.e.,* the cage was rigid with embedded electrodes and fixed to an anchored gantry; however, some geometric error was accumulated from mechanical movements throughout the experiment and human error in determining registration points. To further reduce these errors, we applied a geometric optimization technique to correct the cage location [28]. Briefly, the optimization algorithm iteratively minimized the root-mean-squared error between measured and forward computed potentials on the tank surface by rigidly moving the pericardiac cage. The results presented in this manuscript include examples from both the measured and optimized cage locations.

2.7. Forward problem pipeline

For the forward problem, we selected an epicardial potential source representation and computed the torso-tank surface potentials according to the standard formulation

$$\varphi_{torso} = A\varphi_{cage} \tag{1}$$

where φ_{cage} and φ_{torso} are the vectors of N cage and M torso-tank potentials and A represents an $M \times N$ linear transfer coefficient matrix. For each experiment, A was computed using the boundary element method (BEM) with linear weighting across the triangular elements of the cage and an upsampled, closed version of the torso tank (with 771 nodes) under the assumption of homogeneous torso conductivity [10]. Rows were then extracted from the resultant transfer matrix corresponding to the measured tank electrodes. All these calculations were performed

using boundary element tools in the SCIRun Forward-Inverse Toolkit [26].

2.8. Evaluation of cardiac source sampling

To emulate limited sampling of the cardiac source, we progressively removed horizontal ribs from the pericardiac cage, and their associated recorded signals, starting at the most superior rib and progressing inferiorly (Fig. 4). The associated removed signals were reconstructed using Laplacian interpolation from the remaining signals to mimic standard practice and retain the geometric model and thus the same transfer coefficient matrix.

2.9. Analysis and statistics

Spatial correlation (SC), temporal correlation (TC), and root-mean-square error (RMSE) were used to assess the differences between measured and forward-computed tank potentials. Equations for each metric are as follows:

$$\mathrm{SC} = \frac{1}{N}\sum_{n=1}^{N}\frac{\left(\psi_m(n)-\overline{\psi_m(n)}\right)^T\left(\psi_c(n)-\overline{\psi_c(n)}\right)}{||\psi_m(n)-\overline{\psi_m(n)}||\cdot||\psi_c(n)-\overline{\psi_c(n)}||}$$

$$\mathrm{TC} = \frac{1}{K}\sum_{k=1}^{K}\frac{\left(\chi_m(k)-\overline{\chi_m(k)}\right)^T\left(\chi_c(k)-\overline{\chi_c(k)}\right)}{||\chi_m(k)-\overline{\chi_m(k)}||\cdot||\chi_c(k)-\overline{\chi_c(k)}||} \quad (2)$$

$$\mathrm{RMSE} = \sqrt{\frac{\sum_{k=1}^{K}\sum_{n=1}^{N}\left(\varphi_c\left(k,n\right)-\varphi_m\left(k,n\right)\right)^2}{N\cdot K}}$$

where φ_c and φ_m are $K \times N$ matrices of potentials with K total electrodes and N total time instances. The subscripts m denote measured potentials, and c the calculated potentials. The vector $\psi(n)$ is a vector of the potentials from all electrodes at a time instance n ($\psi(n) = \varphi(:,n)$), and the vector $\chi(k)$ is a vector of the potentials from all time instances from a single electrode k ($\chi(k) = \varphi(k,:)$). $\varphi(k,n)$ denotes a potential value at an electrode k and time n. The values $\overline{\psi}$ and $\overline{\chi}$ denote the mean of those vectors and $||-||$ denotes the 2-norm. The temporal correlation examines the average correlation between the measured and computed signals across all torso electrodes and the spatial correlation examines the average correlation of the torso surface potential distributions across all time points. RMSE was computed over all electrodes and time instants. All three metrics were computed using the entire QRST.

3. Results

3.1. Benchmark forward model accuracy

Measured and forward computed torso potentials from the measured cage location showed close agreement across all beats and experiments. Fig. 5 shows an example of measured, forward computed, and difference potential maps, respectively at the peak of the torso RMS signal (approximately mid-QRS) during a sinus beat. Across all beats, the absolute error was below 15% of the total range of measured potentials and discernible errors were isolated to small regions on the tank surface, as

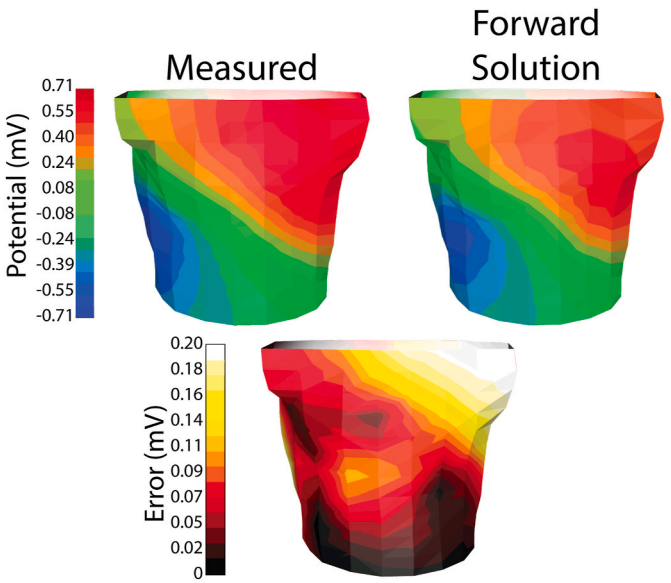

Fig. 5. Example of the measured and computed forward potentials and subsequent difference map during a sinus beat at the peak RMS of the measured potentials. Note the excellent reconstruction of torso potentials and minimal voltage differences.

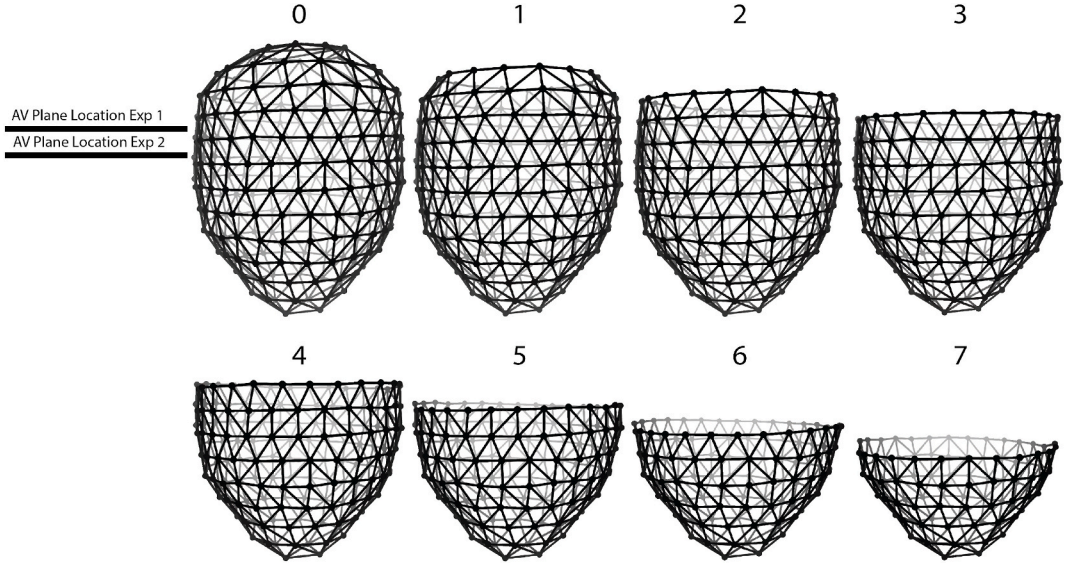

Fig. 4. Pericardiac cage electrode removal pattern that mimics the potential gaps in data collection during experimental preparation using a sock electrode array. Note the removal of cage "ribs" from 0 to 7.

shown in Fig. 5. The difference map shows the highest error anchored in either regions with high potential gradients or the left shoulder region of the tank.

Table 1 shows summary statistics for each beat type across both experiments. All spatial and temporal correlation values were above 0.93, with the highest correlation reaching 0.99. The mean RMSE values across all beat types were low, less than 0.10 mV, which is less than 4% of the average peak to peak signal range and indicates little overall difference in measured vs. computed potential values. In experiment one, ventricularly paced beats from the posterior wall of the heart had 2% lower spatial and temporal correlation values than the ventricular paced beats on the anterior wall.

We also examined the spatial correlation throughout an entire heart beat (Fig. 6). Each plot shows the mean and standard deviation of spatial correlation values across all 40 beats for a different beat type and experiment. Forward computed potentials were less accurate during times of significant temporal gradients, such as the beginning and end of the QRS complex. We also saw oscillations of spatial correlation during the ST-segment segments in sinus beats (Panels C and F in Fig. 6). Across all activation sequence types, we observed spatial correlations consistently above 0.97 during the QRS and T waves.

We also explored the effects of possible geometric error introduced during each experiment using the optimization technique described in section 5.6. For this approach, the pericardiac cage position was corrected on a beat-by-beat basis, which on average translated the cardiac cage by a distance of 15.8 mm ± 2.5 mm and 15.3 mm ± 1.3 mm (mean ± standard deviation) for experiments 1 and 2, respectively. Fig. 7 contains examples of forward computed potentials for both optimized and measured cage positions and their relative differences. Global metrics using the optimized locations are shown in Table 2. The impact of optimizing the location was visible, as shown in Fig. 7 but even in the worst cases, cage optimization only improved spatial and temporal correlation values by 2% (Table 2).

3.2. Evaluation of cardiac source sampling

We examined the effects of removing ribs of electrodes above the AV plane from the measurements of the cardiac source potentials and replacing their values with extrapolated potentials (as shown in Fig. 4) on the resulting computed torso potentials. Figs. 8 and 9 contain examples of computed, measured, and difference potentials following replacement of measured cardiac source signals for each activation sequence type. As expected, the progressive replacement of measured values resulted in increasing error between forward computed and measured potentials. The error increased non-linearly with the number of ribs removed, and the changes varied with activation sequence type. Greater differences for both experiments arose in the superior portions of the torso but varied between anterior or posterior aspects depending on activation sequence.

Figs. 10 and 11 show the summary statistics for each activation sequence and experiment. Replacement of measured signals from the superior cage (top three ribs) produced changes in spatial and temporal correlation coefficients and RMSE values of only −0.05, −0.05, and +0.02 mV, respectively. However reconstruction accuracy decreased precipitously at a specific number of ribs replaced, a number that depended on the experiment. For experiment one, this drop in accuracy was seen when replacing values from the top five ribs, and for experiment two, the top six. Further inspection of photographs taken during the experiments revealed that the sudden drop occurred after replacement of the rib at the approximate level of the atrioventricular (AV) plane; when the cardiac source was sampled only below the AV plane, similar to most epicardial sock recordings, the calculated spatial and temporal correlation values ranged from 0.80 to 0.90. An even more dramatic undersampling resulted in further drops in accuracy, with spatial and temporal correlation coefficients dropping to below 0.50 and RMSE values greater than 0.15 mV after replacing seven ribs with extrapolated values. In both experiments, the ventricular paced beats were less sensitive than the sinus beats to rib replacement in terms of spatial and temporal correlation metrics. By contrast, the trends in RMSE values were more consistent across activation sequence types.

Table 1
Error metrics in forward computed potentials for experiments 1 and 2 using non-optimized cage locations. Each metric is reported as a mean ± standard deviation.

		Mean RMSE (mV)	Mean Spatial Correlation	Mean Temporal Correlation
Exp 1	Ventricular Paced Anterior	0.10±0.003	0.95±0.01	0.98±0.001
	Ventricular Paced Posterior	0.068±0.002	0.95±0.01	0.96±0.005
	Sinus	0.044±0.003	0.93±0.04	0.97±0.006
Exp 2	Ventricular Paced Anterior	0.067±0.004	0.98±0.003	0.99±0.001
	Ventricular Paced Posterior	0.082±0.002	0.98±0.003	0.97±0.002
	Sinus	0.029±0.002	0.93±0.01	0.98±0.003

4. Discussion

4.1. Benchmark forward model accuracy

To our knowledge, this is the most accurate experimentally validated cardiac forward solution in the literature. Our experimental preparation and novel recording arrays limited many sources of error from previous studies. For example, the use of a rigid cage electrode array reduced geometric errors, both for the reconstruction of the electrode locations and elimination of the effects of cardiac contraction. More importantly, the cage contained electrodes over the entire surface and thus ensured more complete sampling of the cardiac source than, *e.g.,* an epicardial sock. We also used a homogeneous volume conductor that removed all effects of torso inhomogeneities, thus reducing another major source of error. As a result of all these measures, our results showed the highest agreement reported to date between computed and measured tank potentials, results that held up across a range of activation sequence types (n = 3 per experiment), across beat to beat variability (n = 40 per activation sequence), and across individual experiments (n = 2). The close agreement is quantified by the spatial correlation, which we used to compare computed and measured body surface recordings at identical time points. This correlation had a peak value of 0.98 and a minimum of 0.93. The temporal correlation, which compares computed and measured torso ECGs through an entire beat, had a peak value of 0.99 and a minimum value of 0.96. Finally, the average RMSE between computed and measured torso electrodes was less than 0.10 mV. The highest error consistently arose in regions with high spatial gradients of potential or during periods of rapid temporal change in the ECG signals. An additional location of relatively higher error was on the left anterior shoulder region of the tank, which was likely caused by the electrical shielding from the experimental perfusion equipment placed in that part of the torso tank. The primary difference in experimental recordings between experiments was a significant increase in noise across all electrodes during experiment one. This difference in noise is likely what caused the variations in correlation and RMSE values across experiments.

Several studies have hypothesized that geometric error acts as one of the most significant contributors to inaccurate forward solutions [27,28]. We controlled for geometric error in our experimental preparation using a rigid cardiac cage, firmly attached to a fixed gantry. To further evaluate the impact of even small geometric errors, we also used a mathematical optimization scheme to adjust the location of the pericardiac cage in the geometric model [28]. In both experiments, the

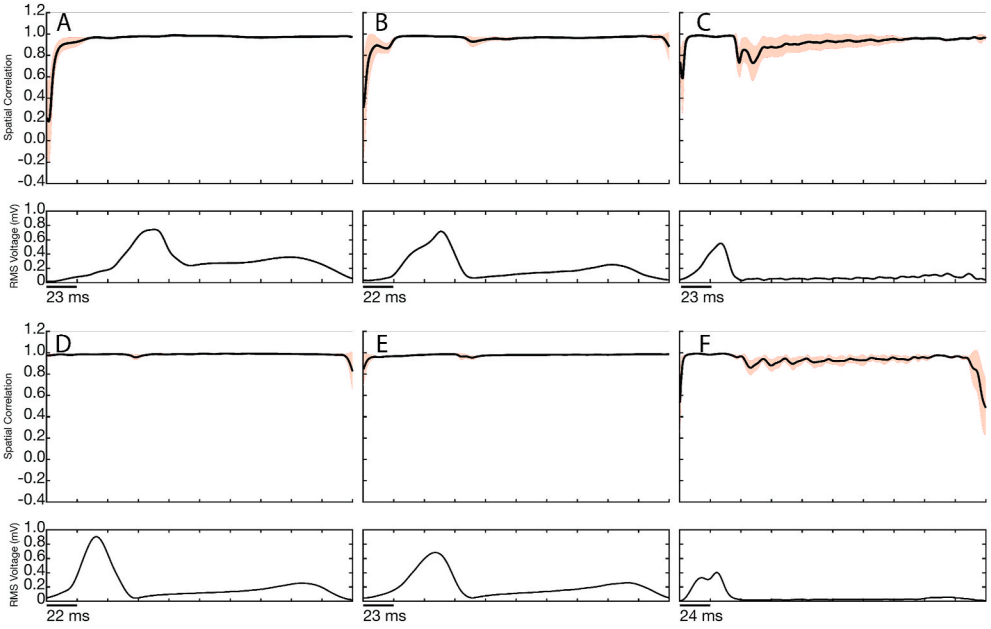

Fig. 6. The spatial correlation variability throughout a recorded beat. Signals are shown as an average across all 40 beats within each type of pacing, time-aligned to a representative beat shown below each correlation signal. Red error bands denote one standard deviation above and below the mean. Panel A: Experiment 1, Anterior ventricular pacing site Panel B: Experiment 1, Posterior ventricular pacing site Panel C: Experiment 1, Sinus beat. Panel D: Experiment 2, Anterior ventricular pacing Panel E: Experiment 2, Posterior ventricular pacing Panel F: Experiment 2, Sinus pacing.

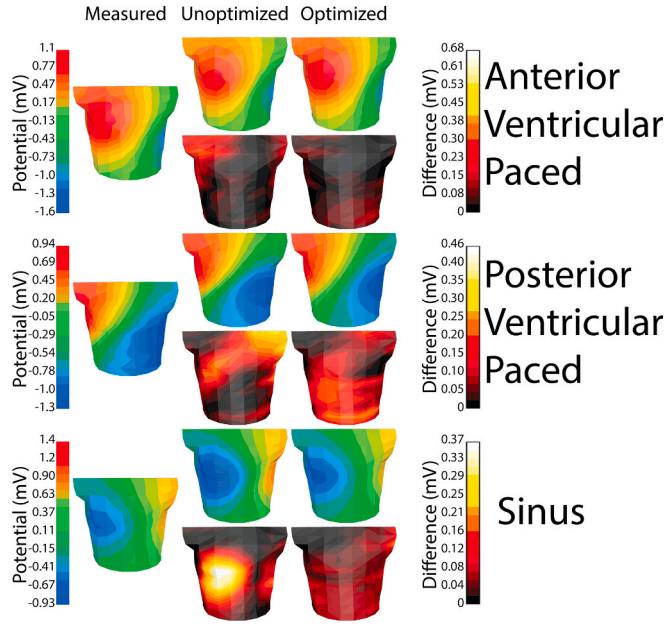

Fig. 7. Example forward computed potentials from three pacing sites using both optimized and measured cage locations from experiment 1. Column one shows the measured torso potentials, column two shows the forward computed potentials using the measured geometry and the difference between measured and forward computation, column three shows the torso potentials using the optimized geometry and the difference between measured and forward computation. The time instant displayed is the peak of the RMS signal within the QRS. Across the three beat types, the spatial correlation coefficients of the measured vs. forward computed torso potentials were for anterior ventricular pacing measured, anterior ventricular pacing optimized, posterior ventricular pacing measured, posterior ventricular pacing optimized, sinus measured, and sinus optimized were 0.96, 0.98, 0.96, 0.96, 0.95, and 0.96, respectively.

optimization moved the pericardiac cage 1.5 cm on average, which is within the range of error that can be explained through possible cage movement during the experiment together with estimated measurement error. This optimization step did not reduce overall error metrics substantially, with the spatial and temporal correlation improving less than

Table 2
Error metrics in forward computing potentials for experiments 1 and 2 using optimized cage locations. Each metric is reported as a mean ± standard deviation.

		Mean RMSE (mV)	Mean Spatial Correlation	Mean Temporal Correlation
Exp 1	Ventricular Paced Anterior	0.047±0.001	0.97±0.02	0.99±0.0005
	Ventricular Paced Posterior	0.056±0.004	0.95±0.02	0.97±0.003
	Sinus	0.032±0.003	0.94±0.04	0.97±0.005
Exp 2	Ventricular Paced Anterior	0.030±0.003	0.99±0.003	0.99±0.001
	Ventricular Paced Posterior	0.028±0.002	0.99±0.003	0.99±0.001
	Sinus	0.017±0.002	0.94±0.01	0.99±0.002

2% and the RMSE error reducing by approximately 0.03 mV, or from 4% to 2% of the peak to peak signal amplitude, which indicates minor changes in RMSE. These minor gains in the quality metrics indicate that the initial geometric reconstructions were sufficiently accurate for subsequent applications of this preparation.

The results of the study also showed that forward solution accuracy with complete source sampling is minimally affected by activation sequence. We hypothesized that ventricularly paced beats would be more accurately reconstructed compared to sinus beats due to the relatively simplicity of activation originating from a single site. Our results, however, showed only very small differences between ventricularly paced and sinus beats (less than 5% correlation and 0.06 mV RMSE). These small differences could be attributed to the increased signal to noise ratio of ventricular paced beats compared to sinus. Additionally, these differences may occur because of the increased complexity of the electrical activation sequence during sinus beats, which we evaluated as an increase in the number of local breakthrough sites identified on the pericardiac cage. Ventricularly paced beats in this study had only one breakthrough site, whereas sinus beats had on average three clearly separate breakthrough sites. Sinus beats have more breakthrough sites because they propagate through the cardiac conduction system, which creates multiple propagating wavefronts throughout the myocardium and thus multiple breakthrough sites.

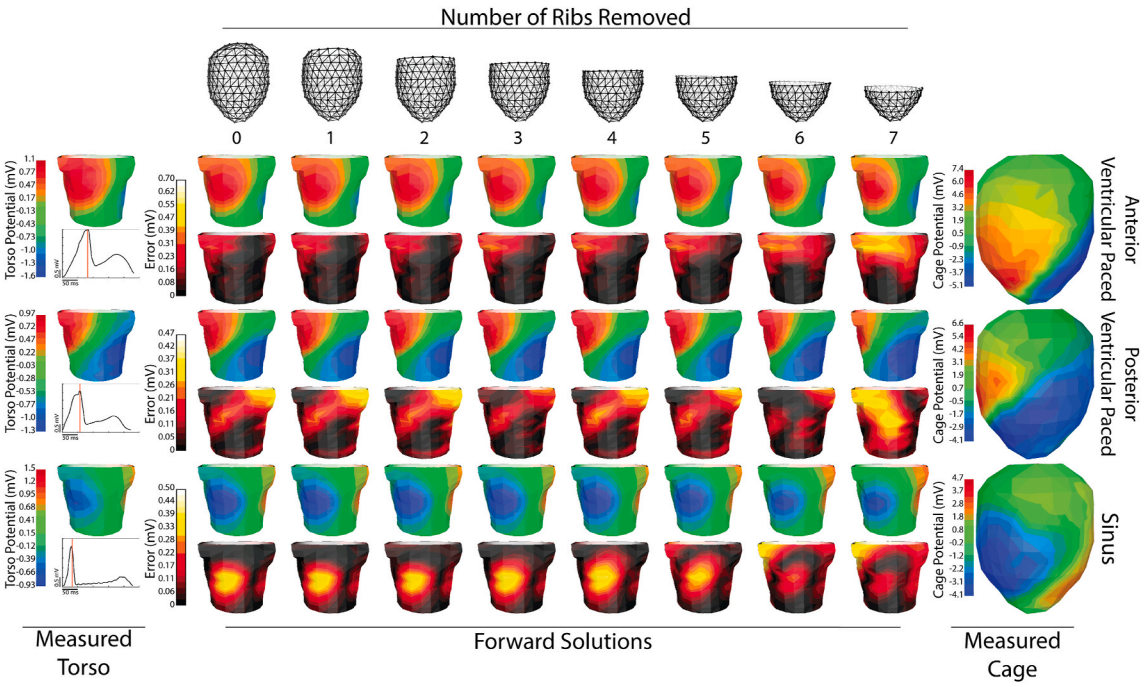

Fig. 8. Experiment #1 summary of results. The first column shows the measured torso surface potential maps. The last column shows the measured cage potentials. All potential maps are shown at the peak of the RMS signal, approximately in the middle of the QRS complex, as denoted by the red line on the RMS curves in column one. The middle columns from left to right show progressive replacement of measured values by extrapolated cage electrograms and subsequent forward-computed potentials and difference maps (with respect to measured potentials) during the peak of the QRS. Each pair of rows shows the forward computed and difference maps for a distinct activation sequence, as labeled on the right-hand side. The torso potential maps use the color bars labeled as 'Torso Potential (mv)' on the left side, the cage potential maps use the color bars labeled as 'Cage Potential (mV)', and difference maps use the color bar labeled 'Error (mV)'.

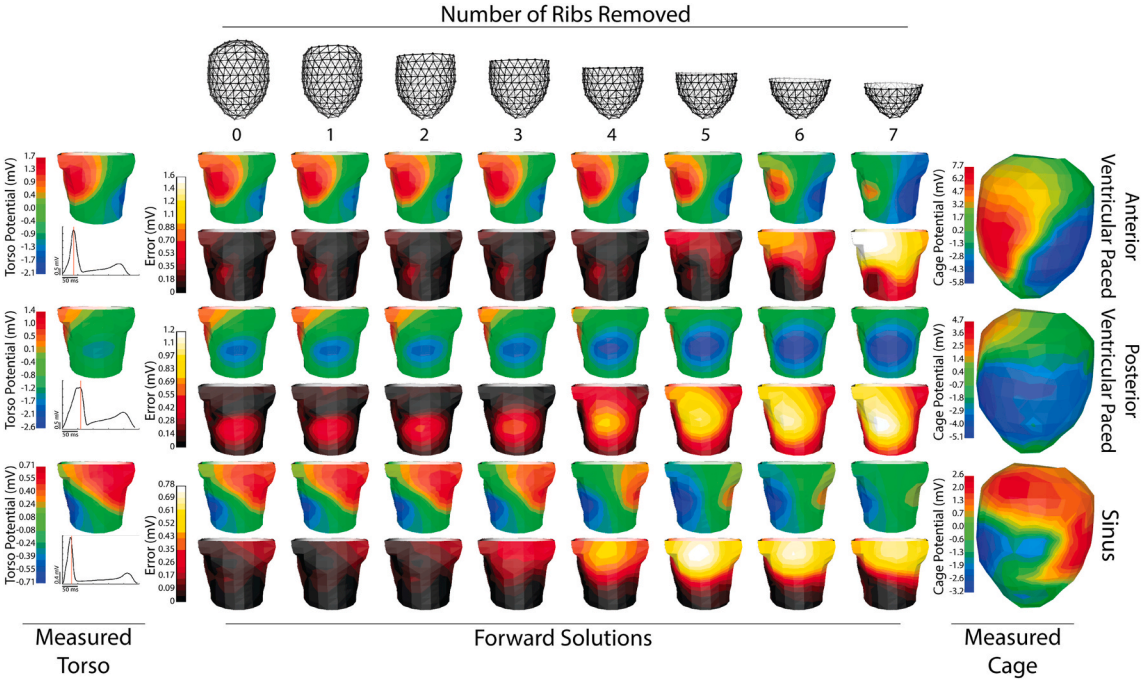

Fig. 9. Experiment #2 summary of results. The organization and layout of the figure are the same as for Fig. 8.

4.2. Evaluation of cardiac source sampling

The recording arrangement also allowed us to test a second hypothesis, that errors in the forward-computed potentials from only ventricular electrograms are a consequence of incomplete cardiac source sampling. By including signals from above the AV plane, we achieved the high accuracy expected from a forward solution *i.e.,* correlation coefficients above 0.95. We also progressively removed rows of measured signals from the pericardiac cage, replaced them with reconstructed (extrapolated) values, and re-computed the tank potentials. There was a precipitous reduction in accuracy when using only measured signals from below the approximate AV plane. This level is

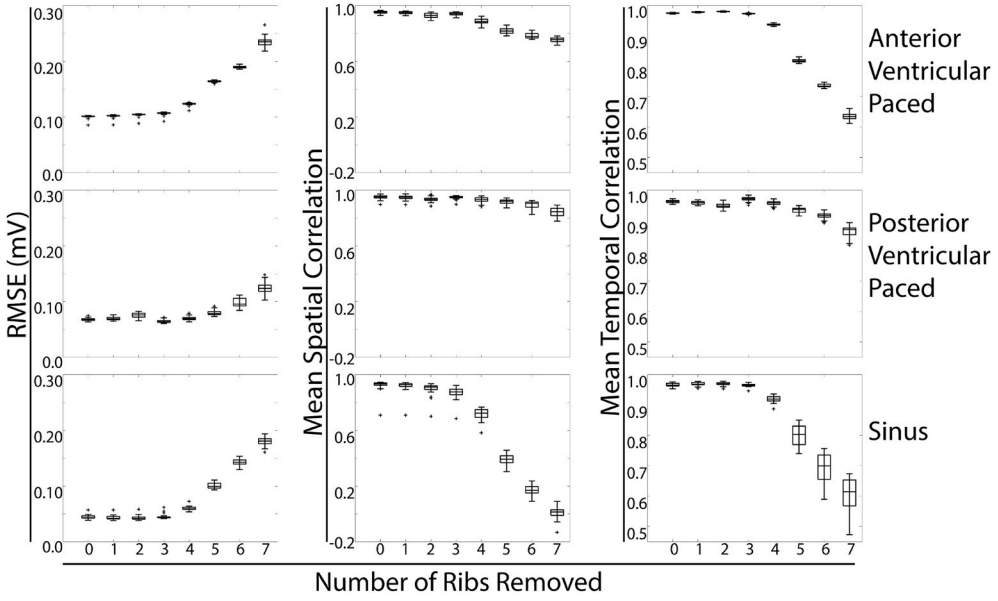

Fig. 10. Experiment #1 statistical summary. The box plots are for each standard accuracy metric with progressive replacement of measured cage potentials in the same manner as described above. The first column shows changes to RMSE values, the second column shows changes to spatial correlation, and the third column shows changes to temporal correlation. The first row shows changes in metrics during anterior ventricular paced, the second row during posterior ventricular paced, and the third row during normal sinus rhythm.

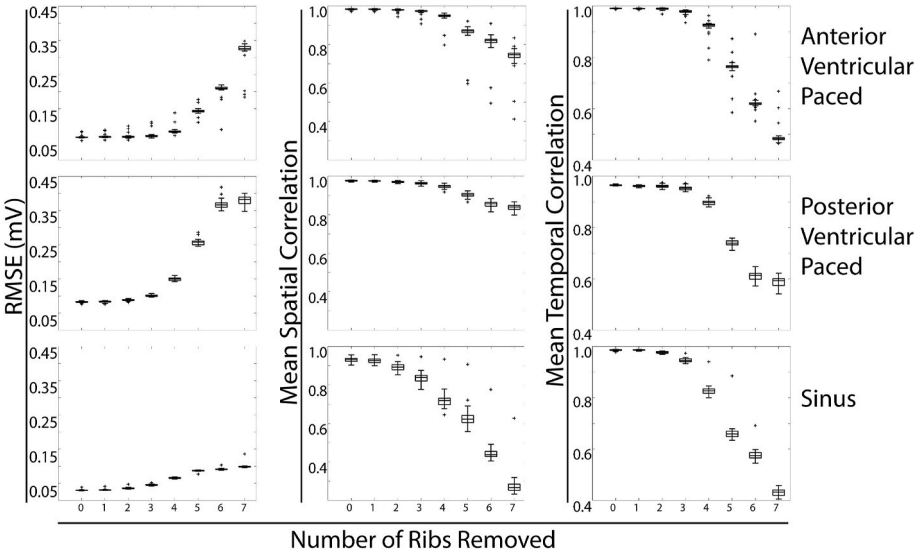

Fig. 11. Experiment #2 statistical summary. The organization and layout of the figure are the same as for Fig. 10.

practically relevant because most experimental recording arrays are ventricular socks, which sample electrical activity primarily from the apex to the AV plane. The remaining potentials needed to create a complete source are reconstructed onto a usually smooth and rounded artificial enclosing surface above the AV plane, a process we replicated using Laplacian extrapolation. The challenges in sampling above the AV plane include anatomical obstacles such as the great vessels, pericardium, and atrial appendages and most studies that have sampled atrial epicardial electrograms have employed a set of small plaque electrodes, which sample densely but with limited coverage [9,29,30]. Using signals below the approximate AV plane produced spatial and temporal correlations between 0.8 and 0.9, substantially worse than when using the complete cage, but within the reported range of previous experimental studies using epicardial sock arrays [8,16]. Our results show that the maximum forward problem accuracy when only sampling ventricular potentials were spatial and temporal correlations below 0.9. Our novel dataset provided a unique opportunity to explore and evaluate more sophisticated reconstruction approaches, studies we have already begun [30].

The errors associated with reduced cardiac sampling corroborate our initial findings based mainly on simulated data. Tate et al. showed that simulated forward potentials were highly inaccurate when samples from the superior aspects of the heart were excluded [9]. Our study is unique because of the novel experimental preparation and validation data with which we isolated the effects of cardiac source sampling. This study is the first experimental validation to produce such an accurate comparison between simulated and recorded torso potentials in multiple experiments and our results suggest that a significant proportion of the forward solution accuracy is dependent on cardiac source sampling.

The clinical implications of our findings are multifaceted and pathology dependent. It is common practice to validate ECGI systems with signals recorded from either the endocardium or epicardium only below the AV plane, based on the assumption that signals from or around the atria are not needed for accurate forward reconstructions. Results from this study clearly dispute this assumption, even for primarily ventricular cardiac activity such as ventricularly paced beats. Additionally, sampling above the AV plane may provide more farfield information to more accurately compute the forward problem. We expect using ECGI systems

that are tuned and validated under this assumption and without complete cardiac sampling will introduce errors that could reduce the accuracy of inverse reconstructions of PVC location, wave re-entry, and other complex arrhythmic events. The consequences will likely be even more problematic in systems developed specifically to characterize atrial arrhythmias, an application that serves as the main driver for commercial ECGI systems.

4.3. Data sharing and availability

To enhance the value and impact of this study for validation of ECGI, we have contributed all the recorded geometric models and processed signals to the Consortium for ECG Imaging (CEI) to make them available for analysis and collaborations. The goal of the CEI is to achieve progress in the field of ECGI through open international collaboration and sharing of ideas, software, and data. The CEI uses a combination of open-source software and a data-sharing platform Experimental Data and Geometric Analysis Repository (EDGAR) (www.edgar.sci.utah.edu) [31] to collaborate across multiple labs and disciplines. Such open collaboration should enable substantially more growth and discovery than when labs work independently. All software used in this study is also available with open-source licensing on the SCI Institute web page.

4.4. Limitations

This study had some limitations. The experimental preparation used an isolated canine heart, which does not fully replicate human physiology, especially with regards to the atria, which are not filled with blood nor do they retain normal function. Additionally, representing the torso volume as a homogeneous isotropic conductive medium does not account for variable electrical conductivities in lung, muscle, and bone, which perturb and modify torso surface potentials. The number and density of the Utah cage electrode array also represents a compromise between sampling accuracy and possible shielding of the cardiac source currents. Perhaps most relevant to its application, the electrograms recorded by the cage do not represent true extracellular surface electrograms as the cage is separated by 1–2 cm from the heart surface. The resulting spatial and temporal smoothing of the recorded signals may improve the accuracy of the ECGI related computations. However, Fig. 8 demonstrates that the measured potentials preserve sufficiently high spatial and temporal resolution for most applications. A final limitation is the number of animal experiments performed (n = 2). The complex nature of these experiments, including the required resources and technical expertise, make them extremely valuable. To add variability to the resulting measurements, we captured multiple beats and applied multiple activation sequences per animal.

5. Conclusion

The results of this study suggest that a substantial portion of errors in forward-computed potentials are a product of inadequate source sampling, which is a typical practice in experimental studies. Our novel experimental preparation provided an ideal dataset to validate this claim and systematically show that comprehensive source sampling is necessary for forward solutions that approach the accuracy expected by the physical, mathematical, and numerical characteristics of this problem. Additionally, this study sets a benchmark for forward solution accuracy by controlling for significant sources of error such as measurement geometry, source sampling, and torso conductivity. The data produced by this study will be available to researchers worldwide and will contribute to further studies to improve methodologies and validate ECGI techniques.

Grant support

Support for this research came from the NIH NHLBI grant no. 1F30HL149327; NIH NIGMS Center for Integrative Biomedical Computing (www.sci.utah.edu/cibc) grant nos. P41GM103545 and R24 GM136986; and the Nora Eccles Treadwell Foundation for Cardiovascular Research.

Declaration of competing interest

WWG: employed by Acutus Medical. All other authors have no other disclosures.

Acknowledgments

We would like to acknowledge the support from the Nora Eccles Treadwell Cardiovascular Research and Training Institute staff, including Jayne Davis, Alicia Booth, Wilson Lobaina and, Bruce Steadman, for preparing and maintaining equipment and coordinating logistics of the experiments.

References

[1] C. Ramanathan, P. Jia, R. Ghanem, K. Ryu, Y. Rudy, Noninvasive electrocardiographic imaging of normal human ventricular activation and repolarization, PANS (2006) vol. in review.
[2] Y. Rudy, B. Lindsay, Electrocardiographic imaging of heart rhythm disorders: from bench to bedside, Card. Electrophysiol. Clin. 7 (2015) 17–35. Mar.
[3] R.N. Ghanem, P. Jia, C. Ramanathan, K. Ryu, A. Markowitz, Y. Rudy, Noninvasive electrocardiographic imaging (ecgi): comparison to intraoperative mapping in patients, Heart Rhythm 2 (4) (2005) 339–354.
[4] L. Bear, I. LeGrice, G. Sands, N. Lever, D. Loiselle, D. Paterson, L. Cheng, B. Smaill, How accurate is inverse electrocardiographic mapping? a systematic in vivo evaluation, Circ Arrhythm Electrophysiol 11 (May 2018), e006108.
[5] M. Cluitmans, D. Brooks, R. MacLeod, O. Doessel, M. Guillem, P.V. Dam, J. Svehlikova, B. He, J. Sapp, L. Wang, L. Bear, Consensus on validation and opportunities of electrocardiographic imaging: from technical achievements to clinical applications, Front. Physiol. 9 (September 2018) 1–19.
[6] P. Cuculich, C. Robinson, Noninvasive ablation of ventricular tachycardia, N. Engl. J. Med. 378 (Apr 2018) 1651–1652.
[7] A. Grace, S. Willems, C. Meyer, A. Verma, P. Heck, M. Zhu, X. Shi, D. Chou, L. Dang, C. Scharf, et al., High-resolution noncontact charge-density mapping of endocardial activation, JCI insight 4 (6) (2019).
[8] L. Bear, L. Cheng, I. LeGrice, G. Sands, N. Lever, D. Paterson, B. Smaill, Forward problem of electrocardiography: is it solved? Circ. Arrhythm. Electrophysiol. 8 (Jun 2015) 677–684.
[9] J. Tate, K. Gillette, B.M. Burton, W. Good, B. Zenger, J. Coll-Font, D. Brooks, R. MacLeod, Reducing error in ECG forward simulations with improved source sampling, Front. Physiol. 9 (2018) 1304.
[10] R. MacLeod, M. Buist, The forward problem of electrocardiography, in: P. Macfarlane, A. van Oosterom, O. Pahlm, P. Kligfield, M. Janse, J. Camm (Eds.), Comprehensive Electrocardiology, Springer Verlag, London, UK, 2010, pp. 247–298.
[11] J. Coll-Font, B. Roig-Solvas, P. van Dam, R.S. MacLeod, D.H. Brooks, Can we track respiratory movement of the heart from the ECG itself - and improve inverse solutions too? J. Electrocardiol. 49 (June 2016) 927.
[12] M. Ramsey, R.C. Barr, M.S. Spach, Comparison of measured torso potentials with those simulated from epicardial potentials for ventricular depolarization and repolarization in the intact dog, Circ. Res. 41 (5) (1977) 660–672.
[13] R. MacLeod, B. Taccardi, R. Lux, The influence of torso inhomogeneities on epicardial potentials, in: IEEE Computers in Cardiology, IEEE Computer Society, 1994, pp. 793–796.
[14] C. Ramanathan, Y. Rudy, Electrocardiographic imaging: I. effect of torso inhomgeneities on body surface electrocardiographic potentials, J. Cardiovasc. Electrophysiol. 12 (Feb. 2001) 229–240.
[15] C. Ramanathan, Y. Rudy, Electrocardiographic imaging: II. effect of torso inhomgeneities on epicardial surface electrocardiographic potentials, J. Cardiovasc. Electrophysiol. 12 (Feb. 2001) 241–252.
[16] M. Cluitmans, P. Bonizzi, J. Karel, M. Das, B. Kietselaer, M. de Jong, F. Prinzen, R. Peeters, R. Westra, P. Volders, In vivo validation of electrocardiographic imaging, JACC Clin Electrophysiol 3 (Mar 2017) 232–242.
[17] S. Schuler, J. Tate, T. Oostendorp, R. MacLeod, O. Dössel, Spatial downsampling of surface sources in the forward problem of electrocardiography, in: Functional Imaging and Modeling of the Heart, Springer-Verlag, Bordeaux, France, 2019, pp. 29–36.
[18] J. Tate, S. Schuler, O. Dössel, R. MacLeod, T.F. Oostendorp, Correcting undersampled cardiac sources in equivalent double layer forward simulations, in: Functional Imaging and Modeling of the Heart, Springer-Verlag, Bordeaux, France, 2019, pp. 147–155.
[19] B. Burton, K. Aras, W. Good, J. Tate, B. Zenger, R. MacLeod, Image-based modeling of acute myocardial ischemia using experimentally derived ischemic zone source representations, J. Electrocardiol. 51 (4) (2018) 725–733.

[20] S. Shome, R. MacLeod, Simultaneous high-resolution electrical imaging of endocardial, epicardial and torso-tank surfaces under varying cardiac metabolic load and coronary flow, in: Functional Imaging and Modeling of the Heart, Lecture Notes in Computer Science, vol. 4466, Springer-Verlag, Berlin, Heidelberg, Germany, 2007, pp. 320–329.
[21] L.R. Bear, Y.S. Dogrusoz, W. Good, J. Svehlikova, J. Coll-Font, E. van Dam, R. MacLeod, The impact of torso signal processing on noninvasive electrocardiographic imaging reconstructions, IEEE Trans. Biomed. Eng. (2020) 1.
[22] D.S. Khoury, B. Taccardi, R.L. Lux, P.R. Ershler, Y. Rudy, Reconstruction of endocardial potentials and activation sequences from intracavitary probe measurements: localization of pacing sites and effects of myocardial structure, Circulation 91 (3) (1995) 845–863.
[23] P. Ershler, R. Lux, B. Steadman, A 128 lead online intraoperative mapping system, in: Proceedings of the IEEE Engineering in Medicine and Biology Society 8th Annual International Conference, IEEE Press, 1986, pp. 1289–1291.
[24] A. Rodenhauser, W. Good, B. Zenger, J. Tate, K. Aras, B. Burton, R. MacLeod, "PFEIFER: preprocessing framework for electrograms intermittently fiducialized from experimental recordings, J. Open Source Software 3 (21) (2018) 472.
[26] B. Burton, J. Tate, B. Erem, D. Swenson, D. Wang, D. Brooks, P. van Dam, R. MacLeod, A toolkit for forward/inverse problems in electrocardiography within the SCIRun problem solving environment, in: Proceedings of the IEEE Engineering in Medicine and Biology Society 33rd Annual International Conference, IEEE Eng. in Med. and Biol. Soc., 2011, pp. 1–4.
[27] D. Swenson, S. Geneser, J. Stinstra, R. Kirby, R. MacLeod, Cardiac position sensitivity study in the electrocardiographic forward problem using stochastic collocation and BEM, Ann. Biomed. Eng. 30 (Dec. 2011) 2900–2910.
[28] J. Coll-Font, D.H. Brooks, Tracking the position of the heart from body surface potential maps and electrograms, Front. Physiol. 9 (2018) 1727.
[29] J.A. Bergquist, W.W. Good, B. Zenger, J.D. Tate, R.S. MacLeod, "GRÖMeR: a pipeline for geodesic refinement of mesh registration, Lect. Notes Comput. Sci. 11504 (2019) 37–45. Functional Imaging and Model of the Heart (FIMH), Springer Verlag.
[30] J. Bergquist, W. Good, B. Zenger, J. Tate, R. MacLeod, Optimizing the reconstruction of cardiac potentials using a novel high resolution pericardiac cage, Comput. Cardiol. 46 (2019) 1–4, 2019.
[31] K. Aras, W. Good, J. Tate, B. Burton, D. Brooks, J. Coll-Font, O. Doessel, W. Schulze, D. Patyogaylo, L. Wang, P. van Dam, R. MacLeod, Experimental data and geometric analysis repository: EDGAR, J. Electrocardiol. 48 (6) (2015) 975–981.